FULL PAPER

Predictive catalysis in olefin metathesis with Ru-based catalysts with annulated C_{60} fullerenes in the N-heterocyclic carbenes

Juan Pablo Martínez,*[a] Miquel Solà,[a] and Albert Poater*[a]

Dedicated to the memory of our colleague Prof. Dr. Victor Snieckus

Abstract: Predictive catalysis must be the tool that does not replace experiments, but acts as a selective agent, so that synthetic strategies of maximum profitability are used in the laboratory in a surgical way. Here, nanotechnology has been mixed with olefin metathesis from homogeneous Ru-NHC catalysts, specifically annulating a C_{60} fullerene to the NHC ligand. Based on results with the C_{60} in the backbone, a sterile change with respect to the catalysis of the metal center, an attempt has been made to bring C_{60} closer to the metal, by attaching it to one of the two C-N bonds of the imidazole group of the SIMes (1,3-bis(2,4,6-trimethylphenyl)imidazolin-2-ylidene) ligand (reference NHC ligand of the 2nd generation Grubbs catalysts) to increase the steric pressure of C_{60} in the first sphere of reactivity of the metal. The DFT calculated thermodynamics and the kinetics of SIMes-derived systems show that they are efficient catalysts for olefin metathesis.

Introduction

The history of olefin metathesis by ruthenium catalysts is closely linked to NHC ligands, which are adopted as a key element once bisphosphine catalysts (1st Generation Grubbs catalysts) are somewhat abandoned and replaced by mixed, phosphine-NHC 2nd Generation Grubbs catalysts.[1,2] At the same time the progress of the ligands has gone in parallel, in fact only 3 decades ago Arduengo reported the synthesis of the first crystalline N-heterocyclic carbon (NHC).[3] And why is there still this hunger to continue modifying olefin metathesis catalysts by means of the NHC ligands?[4] Because these catalysts lead to the generation of carbon-carbon bonds,[5] and no one escapes the importance in which this translates in terms of industrial applications, from the preparation of high value-added molecules for the pharmaceutical industry,[6] biologically active compounds,[7] and on a large scale new materials and polymers.[8]

Having framed the importance of Ru-NHCs for olefin metathesis, it is necessary to know how to focus on the determining steps of the reaction. Thus, of the mechanism first proposed by Chauvin,[9] efforts are being made to emphasize especially the metallacycle,[10] which is its central intermediate that consists of a four-membered ring, including the metal.[11] Any effort to improve the activity of the metallacycle is fundamental, and in fact, such is the importance, that to achieve a minimum relative stability,[12] replacing ruthenium with any other metal led to a complete change of the structure of the ligands around the metal,[13] specially with iron.[14] On the other hand, many studies claim the importance of the preactivation towards the active catalytic 14e species or the release of the substrate.[15,16]

On the other hand, to make a change in the nature of Ru-NHC complexes, one idea is to mix them with nanotechnology, and specifically with C_{60} fullerene. It is not necessary to give many explanations about the importance of C_{60}, as it is included in numerous industrial applications,[17] ranging from the production of solar cells to active agents in the fight against allergies, through its favorable role in trapping radicals.[18] In 2016, some of the present authors analyzed the reaction mechanism of the first combination between C_{60} and Ru-NHC based olefin metathesis catalysts,[19] but in no case was it the first interaction of fullerenes with olefin metathesis, since previously fullerenes had not been part of the NHC ligand, but as substrates in conjunction with norbornene.[20] However, apart from finding a possible support for this type of complexes for improving its activity, its inclusion in the NHC ligand, in its backbone, did not alter the first sphere of the metal in any way. Here, we intend to move one step forward inspired by the work mixing NHC ligands and C_{60} and C_{80} fullerenes.[21,22] Obviously, there are other attempts to mix nanotechnology with organometallic chemistry,[23] but they are still scarce, and special emphasis must be placed on the work of Stang and coworkers on platinum catalysts with macrocycles containing pyrrolidine rings that are linked to C_{60}.[24]

Predictive catalysis is a technique that allows you to make a selection of potential catalysts that improve those present, before their synthesis at the experimental level.[25] Thus, saving the tedious work of synthesizing many of them, and leaving only the focus for which computational chemistry predicts the best properties.[26] Following this strategy, DFT calculations (at the M06/TZVP~sdd//M06L/SVP~sdd level[19,27]) led to modify the ruthenium complexes corresponding to the 2nd Grubbs generation with the SIMes (SIMes = 1,3-bis[2,4,6-(trimethyl)phenyl]imidazolidin-2-ylidene) ligand (**A**). Particularly its backbone was modified by the insertion of a C_{60} molecule (**B** and **C**), replacing directly the methylene H atoms by a fullerene, complex **B**, or both methylene C and H atoms, complex **C**.[19] Here, seeing that catalysts **B** and **C** failed to sterically modify the first sphere around the metal, the potential reactivity of new NHC ligands has been evaluated, where the fullerene is attached to one of the CN bonds of the imidazole ring (see Scheme 1, **D** and **E** complexes). In **D**, the nitrogen atom is replaced by a carbon of

[a] Dr. J. P. Martínez,* Prof. Dr. M. Solà, Dr. A. Poater*
Institut de Química Computacional i Catàlisi and Departament de Química, Universitat de Girona, Campus Montilivi, 17071 Girona, Catalonia, Spain
E-mail: tema_juanpablo@hotmail.com
E-mail: albert.poater@udg.edu

Supporting information for this article is given via a link at the end of the document, absolute energies and Cartesian coordinates.

the fullerene itself, thus changing the methylene group and the contiguous nitrogen and its mesityl by a fullerene, while by **E** only the hydrogens of the methylene group and the mesityl group are replaced by the fullerene.

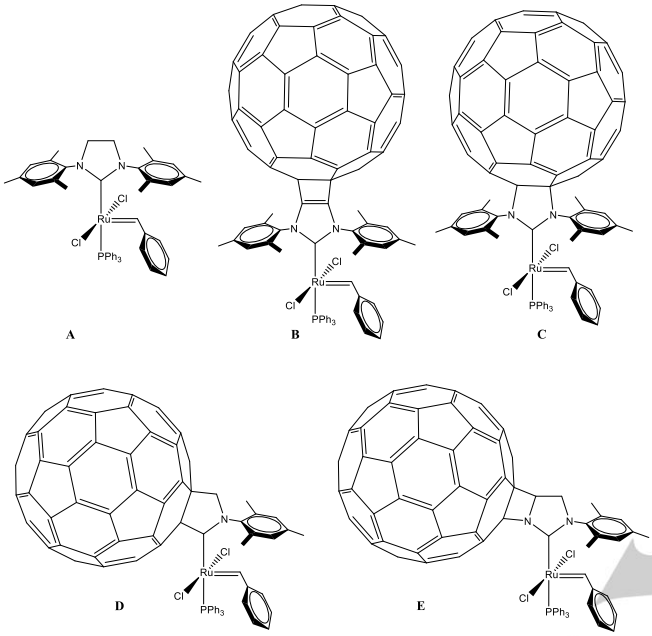

Scheme 1. Ru-based complex with SIMes (1,3-bis(2,4,6-trimethylphenyl)imidazolin-2-ylidene) (**A**) and its *in silico* modifications by the insertion of a C_{60} molecule (**B**-**E**) as olefin metathesis catalysts.

Results and Discussion

The catalytic activities of complexes **A** to **E** are evaluated through the reaction mechanisms corresponding to the olefin metathesis with ethylene as the substrate. The analysis of the thermodynamics and kinetics of the reaction is the main target in the current study, wherein species **I** to **VIII** are quantum-chemically explored (see Scheme 2). Accordingly, Gibbs-energy profiles relative to species **I** for the reaction pathways involving Ru-based complexes are reported in Table 1. The Buckyball C_{60} is linked to the NHC moiety on a pyracylene-type [6,6] bond instead of a corannulene-type [5,6] bond; this configuration is usually the most stable.[28] Indeed, the active catalyst **II** with the [6,6] configuration results in a stabilization of up to 18 kcal/mol as compared to the [5,6] analogue, as previously determined by us.[19]

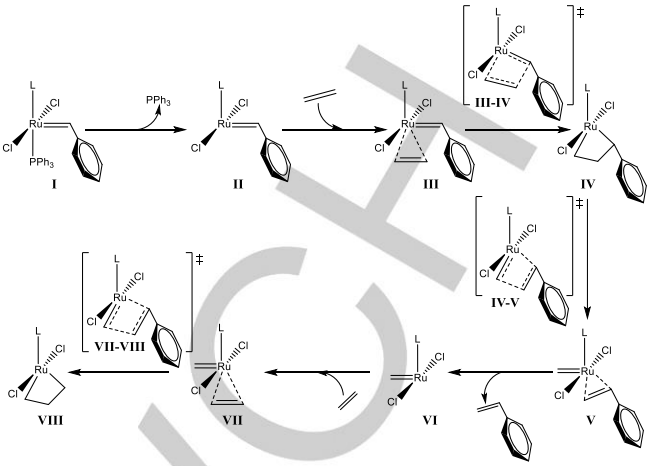

Scheme 2. Olefin metathesis reaction mechanism for Ru based catalysts (L = NHC, phosphine).

Table 1. Computed thermodynamic stability (ΔG in kcal/mol) of the reaction extrema **II**-**VIII** relative to species **I** for the studied olefin metathesis reaction catalyzed by Ru-based complexes **A** to **E** (for **A**-**C** data from Ref. 19), using ethylene as the substrate solvated in CH_2Cl_2.

Complex	A	B	C	D	E
I	0.0	0.0	0.0	0.0	0.0
II	10.5	8.0	12.1	6.9	9.2
III	10.8	10.0	16.2	12.0	10.8
III-IV	15.3	14.5	15.9	13.9	14.7
IV	9.9	8.9	12.6	11.2	13.2
IV-V	17.5	15.1	20.5	18.3	20.0
V	14.9	11.4	16.6	17.7	16.1
VI	13.0	11.1	18.5	16.5	13.1
VII	12.5	10.9	13.4	-	15.5
VII-VIII	13.6	11.0	16.2	-	17.3
VIII	5.3	3.9	7.8	5.9	8.0

The analysis of Table 1 can be conveniently done by introducing the relative thermodynamic stability, ΔΔG, for each intermediate **II** to **VIII** formed by complexes **A** to **E**, which is defined by equation (1).

$$\Delta\Delta G = \Delta G_{complex} - \Delta G_{\mathbf{A}} \quad (1)$$

where the thermodynamic stability of complexes **B** to **E**, $\Delta G_{complex}$, is compared to that of complex **A**, $\Delta G_{\mathbf{A}}$. Moreover, in Table S1 the arithmetic mean of this relative stability, $\overline{X}_{\Delta\Delta G}$, along with the respective standard deviation, $\sigma_{\Delta\Delta G}$, are also calculated to account for the degree of deviation of $\Delta G_{complex}$ related to $\Delta G_{\mathbf{A}}$. In this regard, it is shown that the thermodynamic stability of species **II** to **VIII** via complexes **B** to **E** is nearly identical to the corresponding intermediates formed by complex **A**. For instance, $\overline{X}_{\Delta\Delta G}$ involving species **II** to **VIII** for complex **B** is -1.9 kcal/mol ($\sigma_{\Delta\Delta G}$ = 0.9 kcal/mol); this negative small value of $\overline{X}_{\Delta\Delta G}$ is attributed to the fact that intermediates generated via catalyst **B** are slightly more stable than species of **A**, as can be observed in Table 1.

Besides, ΔΔG is negative in all instances in an energy range of less than 4 kcal/mol, wherein the highest stabilization is reached by **V-B** as compared to **V-A**, ΔΔG = -3.5 kcal/mol. In the cases of **C**, **D**, and **E**, $\bar{X}_{\Delta\Delta G}$ respectively results in 2.7 ($\sigma_{\Delta\Delta G}$ = 1.7), 0.7 ($\sigma_{\Delta\Delta G}$ = 2.3), and 1.4 ($\sigma_{\Delta\Delta G}$ = 1.8) kcal/mol, thus confirming the nearly identical relative stability when compared to **A**. However, ΔΔG is positive for all the intermediates formed through **C**, **D**, and **E** (except for **II-D**, **II-E** and **III-E**) and the transition state **III-IV** for **D** and **E**; therefore, in general species **II** to **VIII** for these catalysts are slightly less stable than species of **A** since 0 < ΔΔG < 6 kcal/mol. Overall, intermediates **III-C** and **VI-C** exhibit the highest destabilization with a ΔΔG of 5.4 and 5.5 kcal/mol, respectively, which is consistent with the kinetically unfavored reaction pathway via catalyst **C**. On the other hand, species **V-B** and **II-D** are the most stabilized intermediates because of a corresponding ΔΔG of -3.5 and -3.6 kcal/mol; indeed, catalysts **B** and **D** show a better performance than the other fullerene-based complexes, thus reflecting the importance of the thermodynamic stabilization of the species formed thru the olefin metathesis.

Although the energy cost of the first step is the largest one regarding the initiation step, to determine the kinetic bottleneck of the reaction pathway it is necessary to look for the barrier of the different TSs with respect to the lowest energy intermediate.[29] In addition, for the first step we omitted the calculation of the energy barrier, if any, since it is a quasi dissociative step.[30,31] The turnover-frequency determining transition state (TDTS) is **IV-V** for all the complexes under study,[32] which corresponds to the opening of the ruthenacyclobutane complex or the [2+2] cycloreversion reaction. After the formation of species **V**, the Gibbs-energy profiles for reaction pathways involving catalysts **A**, **B**, and **D** follow an energetically slight downhill trajectory without high-energy barriers or highly stabilized intermediates, thus resembling previous reports.[33] In fact, the reaction evolves from **VI-D** to **VIII-D** in a barrierless process as determined via a linear-transit calculation (see Figure S1). On the other hand, complexes **C** and **E** does show small energy wells of 2.8 (from **VII-C** to **VII-VIII-C**) and 4.2 kcal/mol (from **VI-E** to **VII-VIII-E**). Overall, the increasing order of the energy barrier calculated via the TDTS follows **B** < **A** < **D** < **E** ≈ **C**, in an energy range from 15.1 to 20.5 kcal/mol. The crucial step in olefin metathesis is the formation of a stable ruthenacyclobutane **IV**, the success of the reaction depends upon this species.[31] Such a structure has been characterized under laboratory conditions.[10] This metallacycle may increase its stability by reducing the number of substituents in the SIMes ligand. Indeed, a poor catalytic performance was observed for the SIMes ligand linked to a phosphine substituent causing the destabilization of the ruthenacyclobutane **IV**. However, a highly stabilized metallacycle could also expose poor catalytic performance.[34] These outcomes allow us to corroborate the relationship between the thermodynamic stability of the ruthenacyclobutane and the potential catalytic activity of the corresponding Ru-catalyst species. In this regard, catalysts **A** to **D** can form a stable metallacycle **IV**. They are stabilized 0.9, 1.1, 3.6, and 0.8 kcal/mol, respectively, when compared to intermediate **III**; these values fitting perfectly with previous results of other active catalysts in olefin metathesis;[35] although species **IV-C** shows the highest stabilization which may be correlated to its kinetically hampered reaction pathway. As a matter of fact, the ruthenacyclobutane is destabilized by 2.4 kcal/mol only in the case of complex **E**, which agrees with the least favored reaction pathway. It is concluded, therefore, that the ruthenacyclobutane should be moderately stable. In particular, catalysts **B** and **D** reveal a catalytic activity comparable to **A** via a moderately stable species **IV**, an attractive outcome for overcoming the drawback of highly stabilized or destabilized metallacycles in olefin metathesis catalysis.

Our results may be additionally explained by analyzing the implications of the Dewar–Chatt–Duncanson framework,[36] wherein the key is the π-backdonation from Ru to the NHC carbene, C_{NHC}. Indeed, electron density donated from the lone pair on nitrogen, N_{NHC}, to C_{NHC} could hamper the π-backdonation leading to complex destabilization related to the formation and dissociation of the ruthenacyclobutane. Those complexes delocalizing electron density around the NHC (a mesomeric-like effect) are thought to hinder the electron density donated from N_{NHC} to C_{NHC}, thus favoring the π-backdonation in a more relaxed process. The highest electron delocalization is predicted for catalyst **B**, as schematized in Figure S2, because more resonance structures are possible. Processes involving formation and rupture of **IV** are, in fact, more stabilized through complex **B** as earlier discussed. Complexes **A**, **C**, and **E** show a similar picture: electron density delocalized through N_{NHC} and C_{NHC}. However, we believe electron density is "pushed" from N_{NHC} to C_{NHC} because of the large π-system in C_{60}, thus leading to complex destabilization via **C** and **E** as compared to **A**. This "pushing" effect may be a consequence of the electron repulsion of π-electrons in C_{60} perpendicular to the electron configuration in the NHC plane. On the contrary, the substitution of N_{NHC} by C_{60}, complex **D**, significantly reduces the number of possible resonance structures, yet fullerene has no lone pair to donate electron density to C_{NHC} such that π-backdonation is relatively less hindered. In fact, most intermediates via catalyst **D** are more stable than the analogous **C** and **E** complexes. ~~In fact, most intermediates via catalyst **D** are more stable than the analogous **C** and **E** complexes~~. Moreover, by performing single-point energy calculations only for the active catalyst fragment at the geometry it acquires to form **IV**, complex **B** and **D** show the most stable HOMO: -140.3 and -141.3 kcal/mol, respectively. Such an outcome supports the premise that electron delocalization and reduction of mesomeric effects around NHC should improve π-backdonation from Ru to C_{NHC}.[37] That is, a stabilized HOMO is originated from better d-π* overlap concerning the metal and NHC moieties. Of course, several orbital contributions are expected to be involved in the π-backdonation and we are omitting those of the olefin as well (its detailed description is beyond the scope of the current work). However, HOMO in the active catalyst

deformed fragment as extracted from **IV** is destabilized by 1.5 in **E**, 4.0 in **A**, and 4.3 in **C** (kcal/mol) as compared to **D**, which may be attributed to a higher electron density donated from N_{NHC} to C_{NHC}. Particularly, in **C** having C_{60} nearer from NHC and resulting in a destabilized metallacycle as early discussed.

Structurally it was also studied how the inclusion of a C_{60} fullerene in the NHC ligand affects in the first sphere of coordination around the metal.[38] The steric maps developed by Cavallo and coworkers[39] provide the index of $\%V_{Bur}$ that is the amount of the first coordination sphere of the metal occupied by a given ligand.[40] We used Samb*V*ca2.1 package[41] to calculate $\%V_{Bur}$. In Table 2, for **E** the values of occupation around the metal because of its NHC ligand were a priori disappointing, with only 29.8% for **I**, and an equidistribution of the four quadrants, never greater than 32.9% for any of them. But these values read in reverse can be the way to have a group that does not tend to decompose as phenyl groups do,[42] like ligands on the imidazole-ring nitrogen. In addition, this catalyst **E** is highly unoccupied around the metal because of its NHC ligand, and therefore the catalyst can use this NHC to interact with sterically highly demanding substrates, and furthermore to avoid any decomposition of the substituent on the imidazole.[42, 43] On the other hand, the $\%V_{Bur}$ for catalyst **D** achieves 35.6% for **I**, and up to 37.5% for the catalytically active species **II**. For the last intermediate, especially, the two values above 40% occupancy of the two quadrants in which the fullerene participates directly are interesting, in particular 41.5 and 41.4%. And this is a detail of being able to almost block sterically impeded substrates. In addition, steric maps in Figure 2 show more clearly than those $\%V_{Bur}$ indices that **D** is more sterically hindered than **A** or **E**, since they depict how the shape of the reactive pocket is modified because of the nature of the NHC ligand. Overall, the decreased $\%V_{Bur}$ for **B** and **E** is a consequence of the fact that being C_{60} attached to NHC makes this ligand more distant from the Ru center. On the other hand, the lowest and highest TDTS result from these complexes such that electronic interactions should also play a significant role.

Table 2. Total $\%V_{Bur}$ and quadrant $\%V_{Bur}$ (Q1, Q2, Q3 and Q4) values for species **I** for the considered Ru-based complexes **A**-**E**.

Complex	Total	Q1	Q2	Q3	Q4
A	33.0	38.2	35.5	31.8	26.7
B	31.9	38.9	31.9	31.2	25.7
C	33.1	35.7	34.7	33.1	29.0
D	35.6	39.4	37.1	34.1	31.4
E	29.8	32.9	30.1	28.7	27.6

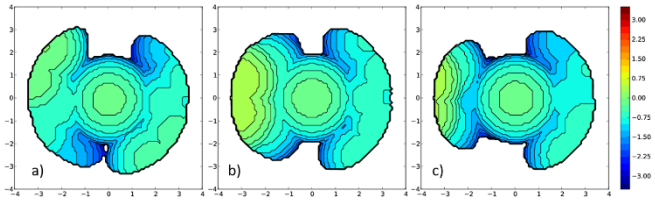

Figure 2. Topographic steric maps (xy plane) of the NHC ligands of species **I** for the studied Ru-complexes a) **A**, b) **D**; and c) **E**. $\%V_{Bur}$ is the percent of buried volume. The Ru atom is at the origin and the C_{NHC} atom is on the z axis, and the 5-membered ring on the xz plane. The isocontour curves of the steric maps are given in Å. The radius of the sphere around the metal center was set to 3.5 Å, while for the atoms we adopted the Bondi radii scaled by 1.17, and a mesh of 0.1 Å was used to scan the sphere for buried voxels.

The effect of the bulky C_{60} fullerene on the binding of NHC to the Ru metal can be quantified by means of the total binding energy, BE,

$$-BE = \Delta E_{strain} + \Delta E_{int} \quad (2)$$

which is evaluated for species **I**-**A** to **I**-**E** (details in Table 3). In equation (2), ΔE_{strain} is the strain energy associated to the change in the geometry of the reactants to the geometry they acquire in species **I**. To our purposes, each complex is divided into the Ru-metal moiety (*f1*, containing the phosphine and benzylidene groups) and the free NHC fragment (*f2*). For complexes **B** to **E**, the NHC counterpart is also linked to C_{60}. Fragments *f1* and *f2* are associated to a strain energy such that ΔE_{strain} equals $\Delta E_{f1,strain}$ plus $\Delta E_{f2,strain}$ for a given complex leading to a positive value, $\Delta E_{strain} > 0$. Table 3 shows that the main contribution to ΔE_{strain} in species **I** is the ruthenium fragment because it is more distorted as compared to the NHC moiety, $8 < \Delta E_{f1,strain} < 13$ and $0 < \Delta E_{f2,strain} < 3$ kcal/mol. In ascending order, ΔE_{strain} follows the sequence **E** < **C** < **B** < **A** < **D** within an energy range of 4 kcal/mol (see relative comparisons in Table 3, rel_{strain}); yet the least strained catalyst **I-E** resulted in the least favored reaction pathway so that electron interactions should play a significant role. Accordingly, we analyze the interaction energy, ΔE_{int}, between the NHC moiety and the metal fragment frozen in the geometry they obtain in the complex. The value of ΔE_{int} is negative since it is the energy gain associated with placing together the two deformed fragments. In ascending order, ΔE_{int} follows the trend **D** < **A** < **E** < **C** < **B** within an energy range of 8 kcal/mol (see relative comparisons in Table 3, rel_{int}). However, catalyst **I-B** exhibits the most favored reaction pathway despite of its less favorable interaction energy. In this regard, the overall effect of strain-interaction is reported by the absolute value of BE, where lower values of ΔE_{strain} and ΔE_{int} increase |BE|, thus representing a more favorable binding between the Ru and NHC fragments. In ascending order, |BE| leads to the sequence **B** < **C** < **E** < **A** < **D** over an energy range of 5 kcal/mol; wherein catalyst **I-B** shows the lowest |BE| although an efficient olefin metathesis is predicted via such a complex. In general, the calculated |BE| is less stabilizing (see the corresponding relative comparison in Table 3, rel_{BE}) for complexes **B** to **E** than that for complex **A** (except for catalyst **I-D** which displays similar |BE| as compared to **I-A**). Therefore, it is concluded that the presence of the C_{60} molecule slightly reduce the strength of the Ru-NHC bond. Furthermore, the trend observed for species **I** regarding |BE| does not provide enough evidence to predict an efficient olefin metathesis; that is, species **I-B** and **I-C** have the lowest |BE| but catalyst **B** shows kinetically favored reaction pathways when compared to catalyst **A**, whereas catalyst **C** disfavors the catalysis when compared to **A**.

Table 3. Strain and interaction energies of species **I**, **III**, **III-IV**, and **IV** for the studied olefin metathesis reaction catalyzed by complex **A** and its *in-silico* modifications with C_{60} annulated NHC backbone, **B** to **E**. Electronic energies in CH_2Cl_2 solvent are given in kcal/mol for the deformation in fragments *f1* (ruthenium moiety) and *f2*, $\Delta E_{f1,strain}$ and $\Delta E_{f2,strain}$, the total strain energy, ΔE_{strain}, the interaction energy, ΔE_{int}, and the total bond energy, BE. A relative comparison (*rel*) is also reported for each parameter under study.

Species	$\Delta E_{f1,strain}$	$rel_{f1,strain}$	$\Delta E_{f2,strain}$	$rel_{f2,strain}$	ΔE_{strain}	rel_{strain}	ΔE_{int}	rel_{int}	|BE|	rel_{BE}
I-A	10.4	0.0	1.9	0.0	12.3	0.0	-61.7	0.0	49.3	0.0
I-B	8.4	-2.0	3.0	1.1	11.4	-0.9	-56.1	5.6	44.7	-4.7
I-C	8.6	-1.8	2.4	0.5	11.0	-1.4	-57.8	3.8	46.9	-2.4
I-D	12.9	2.4	1.4	-0.4	14.3	2.0	-64.1	-2.5	49.8	0.5
I-E	9.6	-0.8	0.6	-1.3	10.2	-2.1	-58.3	3.3	48.1	-1.3
III-A	2.8	0.0	1.6	0.0	4.4	0.0	-18.9	0.0	14.5	0.0
III-B	11.2	8.5	5.2	3.5	16.4	12.0	-29.9	-11.0	13.5	-1.0
III-C	13.5	10.7	5.4	3.7	18.9	14.5	-31.9	-13.0	13.1	-1.4
III-D	2.0	-0.8	1.2	-0.4	3.1	-1.2	-16.2	2.7	13.0	-1.5
III-E	4.3	1.6	2.5	0.9	6.9	2.5	-20.3	-1.4	13.4	-1.1
III-IV-A	15.5	0.0	12.5	0.0	28.0	0.0	-40.3	0.0	12.3	0.0
III-IV-B	16.1	0.6	13.2	0.7	29.3	1.3	-41.7	-1.3	12.3	0.0
III-IV-C	14.4	-1.1	11.6	-0.9	26.0	-2.0	-39.7	0.7	13.7	1.4
III-IV-D	15.5	0.0	13.4	0.9	28.9	0.9	-39.6	0.8	10.7	-1.6
III-IV-E	18.1	2.5	13.3	0.8	31.3	3.3	-41.8	-1.5	10.5	-1.9
IV-A	56.2	0.0	53.9	0.0	110.0	0.0	-127.8	0.0	17.8	0.0
IV-B	58.0	1.8	54.1	0.2	112.1	2.1	-129.4	-1.6	17.3	-0.5
IV-C	52.2	-3.9	52.9	-1.0	105.2	-4.9	-124.1	3.8	18.9	1.1
IV-D	57.6	1.4	53.7	-0.2	111.3	1.3	-127.8	0.0	16.5	-1.3
IV-E	60.3	4.1	55.3	1.4	115.5	5.5	-130.2	-2.4	14.7	-3.1

Alluding to the activation strain model (ASM),[44] the first step of the reaction is also analyzed in an attempt to stablish a relationship between reaction barriers and the properties of the catalytic active species **II**; as well as the characteristics of the reaction mechanisms. Due to the breaking of the ruthenacyclobutane, the ASM starting from species **II** cannot be applied to the TDTS described by **IV**-**V**. Consequently, we focus on the energy barriers related to the closure of the metallacycle, species **III-IV**, to provide a comprehensive analysis about how the balance between sterics and electronics drives to the metallacycle.[45] Accordingly, to apply equation (2) considering the previous strain-interaction scheme, species **III**, **III-IV**, and **IV** are divided into the Ru metal fragment, *f1* which corresponds to species **II**, and the ethylene moiety, that is *f2*. Species **III** is formed by the coordination between the active catalyst **II** and ethylene, thus causing a structural deformation in both fragments denoted as $\Delta E_{f1,strain}$ and $\Delta E_{f2,strain}$. Table 3 reports the energy costs related to $\Delta E_{f1,strain}$, $\Delta E_{f2,strain}$, and ΔE_{strain} in species **III**; for these three parameters the distortion increases in the order **D** < **A** < **E** < **B** < **C** in an energy range of 16 kcal/mol (see rel_{strain}). In contrast, the inverted ascending sequence is observed for ΔE_{int}. Subsequently, intermediate **III-D** results in the lowest strain energy, yet its electron interactions are also the least favored ones. Nevertheless, |BE| (ca. 14 kcal/mol) is nearly identical for all complexes, being **III-A** slightly favored by less than 2 kcal/mol as reported by rel_{BE}. Therefore, we investigate the transition state to grasp a better understanding about how the formation of the metallacycle affects the reaction.

The energy costs associated to ΔE_{strain} in the transition state **III-IV** follow an ascending order of **C** < **A** < **D** < **B** < **E** within an energy range of less than 6 kcal/mol (see rel_{strain}). Both $\Delta E_{f1,strain}$ and $\Delta E_{f2,strain}$ show to some extent similar trends, where the lowest distortion in each fragment is also calculated for **III-IV-C**. On the other hand, the ascending sequence for ΔE_{int} is **E** < **B** < **A** < **C** < **D** for a small energy range of only 3 kcal/mol (see rel_{int}).[46] The relative lower strain and higher electron interactions for species **III-IV-C** leads to a more favored |BE|, whereas the less favored |BE| corresponds to **III-IV-E**. However, given that rel_{BE} is within a small energy range of 3 kcal/mol regarding complexes **A** to **E**, our analysis is not conclusive at all since both complexes **C** and **E** show the highest energy barriers (also the highest TDTS). Consequently, we now investigate the metallacycle, species **IV**, to describe the performance of the catalysts in olefin metathesis. Even though **IV-C** is once again the least distorted intermediate since $\Delta E_{f1,strain}$ and ΔE_{strain} follow the ascending-order sequence **C** < **A** < **D** < **B** < **E** within an energy range of less than 11 kcal/mol ($\Delta E_{f2,strain}$ slightly differs from this series), its ΔE_{int} is also the least favored one. Like the analysis for **III-IV**, species **IV-E** shows once again the highest strain and the best electron interactions. The ascending series of |BE| for species **IV** is also identical to that of **III-IV**, **E** < **D** < **B** < **A** < **C**. On the one hand complex **E** leads to the lowest |BE| for both the metallacycle and its forming transition state because of high structural deformation despite of better electron interactions. On the other hand, complex **C** exposes the highest |BE| for both species due to low structural strain, despite poorer electron interactions. Our calculations suggest that structural deformation mainly drives |BE| for species **III-IV** and **IV**. More importantly, the fact that complexes **C** and **E**, which exhibit the least favored reaction pathways, result in the highest and lowest |BE|, respectively, confirms our previous conclusion: the metallacycle should be moderately stabilized. In terms of the analysis attained by means of the ASM, the |BE| of the ruthenacyclobutane complex formed via catalysts **A**, **B**, and **D** is neither the highest nor the lowest one; then it is concluded that |BE| is moderate and it is corroborated by comparing the corresponding Gibbs energy between **III** and **IV**, which differs by 1 kcal/mol as previously mentioned. In addition, Table 1 also shows that species **IV-C** is stabilized by 3.6 kcal/mol compared to **III-C** leading to the highest |BE|, but **IV-E** is destabilized by 2.5 kcal/mol resulting in the lowest |BE|.

Table 4. Electronic properties of species **I** and **II** for the considered Ru-complexes **A** to **E**. Ruthenium-carbene bond distance d_{Ru-C} in Å, natural charges in ruthenium, q_{Ru}, and the carbene, q_C, in e^-. Energies of the HOMO (ε_H), the LUMO (ε_L), chemical hardness (η), chemical potential (μ), and Parr electrophilicity index (ω) in kcal/mol. Respective arithmetic mean and standard deviation are also reported.

Species	d_{Ru-C}	q_{Ru}	q_C	ε_H	ε_L	η	μ	ω
I-A	2.06	-0.36	0.49	-126.91	-48.29	39.31	-87.60	97.60
I-B	2.07	-0.38	0.43	-129.61	-50.34	39.63	-89.97	102.12
I-C	2.07	-0.36	0.51	-126.78	-52.02	37.38	-89.40	106.91
I-D	2.00	-0.34	0.42	-131.15	-52.59	39.28	-91.87	107.42
I-E	2.04	-0.37	0.40	-127.10	-49.65	38.72	-88.38	100.85
$\bar{X}$	2.05	-0.36	0.45	-128.31	-50.58	38.87	-89.44	102.98
σ	0.03	0.02	0.05	1.97	1.75	0.89	1.63	4.17
II-A	1.93	-0.03	0.55	-137.39	-53.71	41.84	-95.55	109.10
II-B	1.93	-0.01	0.48	-134.52	-55.19	39.66	-94.85	113.42
II-C	1.93	-0.02	0.56	-139.26	-55.72	41.77	-97.49	113.76
II-D	1.89	-0.01	0.45	-144.21	-59.16	42.53	-101.68	121.56
II-E	1.92	0.01	0.46	-135.59	-52.15	41.72	-93.87	105.59
$\bar{X}$	1.92	-0.01	0.50	-138.20	-55.18	41.51	-96.69	112.69
σ	0.02	0.01	0.05	3.82	2.62	1.08	3.09	5.99

We include an additional analysis to provide a deeper understanding of the subject. We report the bond distance between ruthenium and the carbene (d_{Ru-C}) for the catalyst **I** and the active catalyst **II** in Table 4, as well as the natural charges of ruthenium, q_{Ru}, and the carbene, q_C. No significant differences are found since the bond-distance arithmetic mean equals 2.05 Å (σ = 0.03 Å) for species **I** and 1.92 Å (σ = 0.02 Å) in the case of species **II**. Moreover, the catalysts **A** to **E** show quite similar q_{Ru}, the arithmetic mean is calculated to be -0.36 e^- (σ = 0.02 e^-) for species **I** and -0.01 e^- (σ = 0.01 e^-) in the case of species **II**. A slightly larger difference (σ increases) is observed for q_C among complexes **A** to **E**, it results in an arithmetic mean of 0.45 e^- (σ = 0.05 e^-) for **I** and 0.50 e^- (σ = 0.05 e^-) for **II**. Overall, the release of the phosphine group from **I** to form the active catalyst **II** causes a

reduction in d_{Ru-C} and a more positive-charged ruthenium to attract the electrons of the olefin. However, the observed similarities do not provide enough evidence to correlate the catalytic activity in olefin metathesis. Therefore, we performed an additional conceptual DFT analysis to achieve a comprehensive insight into the electronic contribution of the NHCs.

The electrophilicity of the complexes is therefore evaluated via the Parr electrophilicity index shown in equation (3),[47]

$$\omega = \frac{\mu^2}{2\eta} \qquad (3)$$

here μ and η respectively stand for the chemical potential and the molecular hardness, which are defined as the first and second derivatives of the energy with respect to N at a fixed external potential, given an N-electron system with total electronic energy E.[48] Assuming the validity of the Koopmans' approximation,[49] μ and η are evaluated by equation (4),

$$\mu \cong \frac{1}{2}(\varepsilon_L + \varepsilon_H) \quad and \quad \eta \cong \frac{1}{2}(\varepsilon_L - \varepsilon_H) \qquad (4)$$

with ε_H and ε_L as the energies of the highest occupied molecular orbital (HOMO) and the lowest unoccupied molecular orbital (LUMO), respectively. These values along with ω, μ, and η for the species **I** and **II** are reported in Table 4. Figure 3a schematizes the HOMO and LUMO in complex **A**, but such a configuration is not the same for the rest of the catalysts; then we look for appropriate frontier molecular orbitals to calculate the electronic properties under consideration. In fact, the selected frontier orbitals were usually HOMO and LUMO+3 for **B** to **E** (see Figure 3b and Table S2). In the case of species **I**, ε_H and ε_L result in an arithmetic mean of -128.3 and -50.6 kcal/mol, respectively, with no significant variations among the complexes because of a standard deviation σ < 2 kcal/mol. The resistance of a system to change in the number of electrons is evaluated via η, and the energy released when the number of electrons increase due to a more accessible LUMO is assessed by μ. The fact that ε_H and ε_L slightly vary thru species **I-A** to **I-E** leads to small variations in η and μ which is reflected in the corresponding σ value of less than 2 kcal/mol. In view of the square of μ in equation (3), the arithmetic mean of ω equivalent to 103.0 kcal/mol reveals higher deviations reported by σ = 4.2 kcal/mol. The higher electrophilicity of fullerene-based catalysts as compared to **I-A** is attributed to their slightly higher μ, hence complexes **I-B** to **I-E** may be more reactive to nucleophilic attacks.[50] In the case of the active catalyst, species **II**, the arithmetic means of ε_H and ε_L show higher variations, 2 < σ < 4 kcal/mol. However, these fluctuations do not have an impact in η since σ = 1.1 kcal/mol; indeed, the higher value of η in **II** ($\bar{X}$ = 41.5 kcal/mol) as compared to **I** ($\bar{X}$ = 38.9 kcal/mol) is attributed to a higher electron stabilization for the active catalyst, an advantageous prerequisite to undergo olefin metathesis. Higher deviations are calculated for μ (σ = 3.1 kcal/mol) and, as a result, for ω (σ = 6.0 kcal/mol). Even though we could not find out clear trends based on these later quantities, in general we can conclude that a reduced electron donating capability of the SIMes ligand with a backbone annulated by a C_{60} molecule, that is hard chemical species along with an increased electrophilicity, should provide insights to investigate this new family of catalysts in an attempt to solve bottlenecks in olefin metathesis.

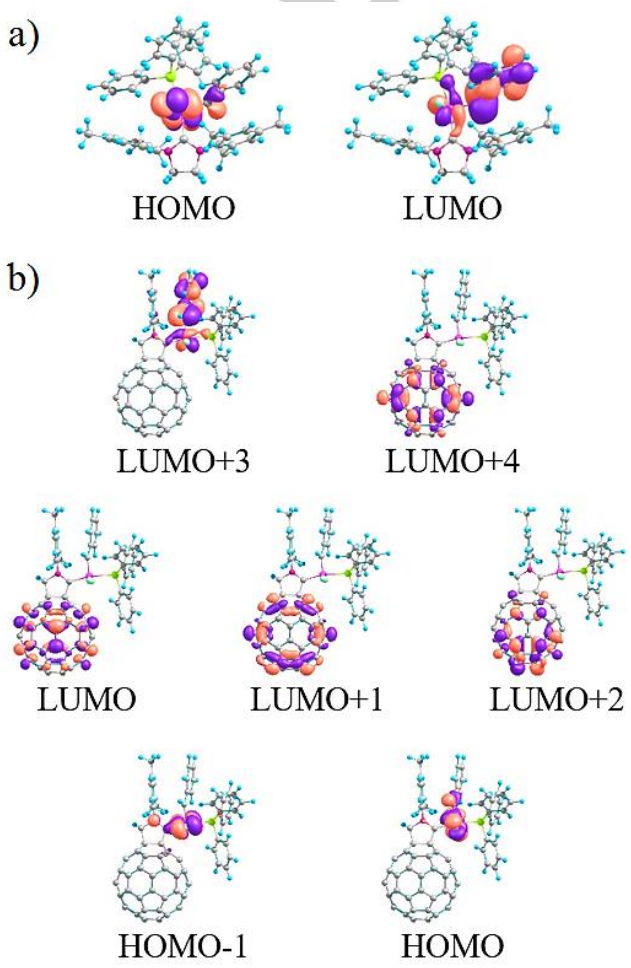

Figure 3. Frontier molecular orbitals for a) Ru-based complex **I-A**, and b) *in-silico* modified catalyst **I-D**.

Conclusions

DFT calculations have been the way to predict Ru(NHC) catalysts with a C_{60} molecule annulated in the SIMes ligand, not simply to join organometallics with nanotechnology, but to make the fullerene simultaneously an active actor in the first sphere around the metal, also protecting the mesityl group potential decomposition catalyst itself from the imidazole ring. Kinetically and thermodynamically the new catalysts proposed for predictive catalysis do not report any drawbacks, and even the catalyst where the fullerene exchanges one of the two nitrogen atoms of the imidazole ring for a carbon, has a slightly improved kinetics for the closure of the metallacycle compared to the reference

SIMes, unmodified. In addition, once the metallacycle is opened, the resulting olefin release would prove to be more favorable than with any other system. Thus, the inclusion of a C_{60} in the NHC ligand near the metal center of an Ru-NHC is promising in order to improve olefin metathesis. It should be clarified here that our study on predictive catalysis uses ligands that could be challenging for current synthetic chemistry, but may guide future synthetic efforts that can improve olefin metathesis.[51]

.

Experimental Section

DFT calculations were carried out with the Gaussian09 set of programs.[52] The M06L functional was employed in geometry optimizations and frequency calculations,[53] while for the electronic configuration of the molecular systems the standard split-valence basis set with a polarization function of Ahlrichs and co-workers for H, C, N, and Cl was used (SVP keyword in Gaussian09).[54] In particular, for Ru we used the small-core, quasi-relativistic Stuttgart/Dresden effective core potential, with an associated valence basis set contracted (standard SDD keywords in Gaussian09).[55] The geometry optimizations were carried out without symmetry constraints, and the characterization of the located stationary points was performed by analytical frequency calculations. Using the zero point energy and thermal and entropic corrections from the gas phase frequency calculations at the M06L/SVP level of theory, Gibbs energies, ΔG, were generated through single point energy calculations on the M06L/SVP geometries using the M06 functional and the triple-ζ valence plus polarization on main group atoms (TZVP keyword in Gaussian),[56] including the solvent effects with the PCM model using CH_2Cl_2 as the solvent.[57]

Acknowledgements

J.P.M. gratefully acknowledges the receipt of his Ph.D. fellowship (register/application number 217067/312543) financed by the Mexican CONACYT. A.P. is a Serra Húnter Fellow. We are grateful to the Ministerio de Economía y Competitividad (MINECO) of Spain for projects CTQ2017-85341-P and PGC2018-097722-B-I00; Generalitat de Catalunya for project 2017SGR39, Xarxa de Referència en Química Teòrica i Computacional, and ICREA Academia prize 2019 to A. P.

Keywords: fullerene • olefin metathesis • DFT calculations • metallacycle • ruthenium • SIMes • NHC

References

FULL PAPER

Entry for the Table of Contents

FULL PAPER

Annulating C_{60} fullerenes in NHC ligands enhances the catalysis of Ru-based olefin metathesis catalysis.

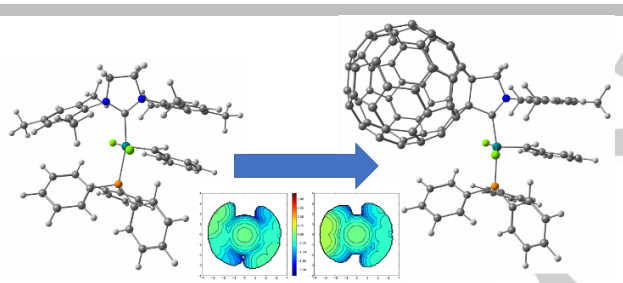

J. P. Martínez, M. Solà, and A. Poater**

Page No. – Page No.
Predictive catalysis in olefin metathesis with Ru-based catalysts with annulated C60 fullerenes in the N-heterocyclic carbenes

[1] a) J. A. Tallarico, P. J. Bonitatebus, Jr.; M. L. Snapper, *J. Am. Chem. Soc.* **1997**, *119*, 7157-7158; b) D. R. Anderson, D. D. Hickstein, D. J. O'Leary, R. H. Grubbs, *J. Am. Chem. Soc.* **2006**, *128*, 8386-8387; c) C. Adlhart, P. Chen, *J. Am. Chem. Soc.* **2004**, *126*, 3496-3510.

[2] a) T. Weskamp, W. C. Schattenmann, M. Spiegler, W. A. Herrmann, *Angew. Chem. Int. Ed.* **1998**, *37*, 2490-2493; b) J. Huang, E. D. Stevens, S. P. Nolan, J. L. Petersen, *J. Am. Chem. Soc.* **1999**, *121*, 2674-2678; c) M. Scholl, S. Ding, C. W. Lee, R. H. Grubbs, *Org. Lett.* **1999**, *1*, 953-956; d) F. B. Hamad, T.-L. Sun, S.-Q. Xiao, F. Verpoort, *Coord. Chem. Rev.* **2013**, *257*, 2274-2292.

[3] A. J. Arduengo, R. L. Harlow, M. Kline, *J. Am. Chem. Soc.* **1991**, *113*, 361-363.

[4] a) F. Nahra, D. J. Nelson, S. P. Nolan, *Trends Chem.* **2020**, *2*, 1096-1113; b) Q. Zhao, G. Meng, S. P. Nolan, M. Szostak, *Chem. Rev.* **2020**, *120*, 1981-2048.

[5] a) R. H. Grubbs, Handbook of Metathesis: Catalyst Development, Wiley-VCH, Weinheim, Germany, 2003; b) G. C. Vougioukalakis, R. H. Grubbs, *Chem. Rev.* **2010**, *110*, 1746-1787; c) C. Samojłowicz, M. Bieniek, K. Grela, *Chem. Rev.* **2009**, *109*, 3708-3742; d) A. Fürstner, *Angew. Chem., Int. Ed.* **2000**, *39*, 3012-3043; e) B. K. Keitz, K. Endo, P. R. Patel, M. B. Herbert, R. H. Grubbs, *J. Am. Chem. Soc.* **2012**, *134*, 693-699.

[6] a) S. J. Connon, S. Blechert, *Angew. Chem. Int. Ed.* **2003**, *42*, 1900-1923; b) F. Pozgan, P. H Dixneuf, Metathesis Chemistry: From Nanostructure Design to Synthesis of Advanced Materials, Springer, Dordrecht, The Netherlands, 2007, vol. 243, pp. 195-222.

[7] B. K. Keitz, R. H. Grubbs, *Organometallics* **2010**, *29*, 403-408.

[8] a) A. Leitgeb, J. Wappel, C. Slugovc, *Polymer* **2010**, *51*, 2927-2946; b) C. W. Bielawski, R. H. Grubbs, *Prog. Polym. Sci.* **2007**, *32*, 1-29; c) J. C. Mol, *J. Mol. Catal. A: Chem.* **2004**, *213*, 39-45.

[9] P. J. L. Hérisson, Y. Chauvin, *Die Makromol. Chem.* **1971**, *141*, 161-176.

[10] a) P. E. Romero, W. E. Piers, *J. Am. Chem. Soc.* **2007**, *129*, 1698-1704; b) E. F. van der Eide, W. E. Piers, *Nat. Chem.* **2010**, *2*, 571-576; b) L. Cavallo, *J. Am. Chem. Soc.* **2002**, *124*, 8965-8973; f) A. Correa, L. Cavallo, *J. Am. Chem. Soc.* **2006**, *128*, 13352-13353.

[11] a) A. D. Kulkarni, D. G. Truhlar, *J. Chem. Theory Comput.* **2011**, *7*, 2325-2332; b) Y. Zhao, D. G. Truhlar, *J. Chem. Theory Comput.* **2009**, *5*, 324-333; c) Y. Zhao, D. G. Truhlar, *Org. Lett.* **2007**, *9*, 1967-1970; d) Y. Zhao, D. G. Truhlar, *Chem. Phys. Lett.* **2011**, *502*, 1-13; e) Y. Zhao, D. G. Truhlar, *Acc. Chem. Res.* **2008**, *41*, 157-167; f) G. Occhipinti, H.-R. Bjørsvik, V. R. Jensen, *J. Am. Chem. Soc.* **2006**, *128*, 6952-6954; g) Y. Minenkov, A. Singstad, G. Occhipinti, V. R. Jensen, *Dalton Trans.* **2012**, *41*, 5526-5541; h) A. C. Tsipis, A. G. Orpen, J. N. Harvey, *Dalton Trans.* **2005**, 2849-2858; i) G. Occhipinti, F. R. Hansen, K. W. Törnroos, V. R. Jensen, *J. Am. Chem. Soc.* **2013**, *135*, 3331-3334; j) P. Tobón, S. Gómez, A. Restrepo, F. Núñez-Zarur, *Organometallics* **2021**, 40, 119-133.

[12] a) N. B. Nechmad, R. Phatake, E. Ivry, A. Poater, N. G. Lemcoff, *Angew. Chem. Int. Ed.* **2020**, *59*, 3539-3543; b) G. Segalovich-Gerendash, I. Rozenberg, N. Alassad, N. B Nechmad, I. Goldberg, S. Kozuch, N G. Lemcoff, *ACS Catal.* **2020**, *10*, 4827-4834.

[13] a) J. A. Luque-Urrutia, M. Gimferrer, E. Casals-Cruañas, A. Poater, *Catalysts* **2017**, *7*, 389; b) A. Poater, S. V. C. Vummaleti, E. Pump, L. Cavallo, *Dalton Trans.* **2014**, *43*, 11216-11220.

[14] D. S. Belov, Logesh Mathivathanan, M. J. Beazley, W. B. Martin, K. V. Bukhryakov, *Angew. Chem. Int. Ed.* **2021**, 60, 2934-2938.

[15] a) M. Barbasiewicz, A. Szadkowska, R. Bujok, K. Grela, *Organometallics* **2006**, *25*, 3599-3604; b) X. Bantreil, A. Poater, C. A. Urbina-Blanco, Y. D. Bidal, L. Falivene, R. A. M. Randall, L. Cavallo, A. M. Z. Slawin, C. S. J. Cazin, *Organometallics* **2012**, *31*, 7415-7426; c) C. Costabile, A. Mariconda, L. Cavallo, P. Longo, V. Bertolasi, F. Ragone, F. Grisi, *Chem. Eur. J.* **2011**, *17*, 8618-8629; d) F. Núñez-Zarur, X. Solans-Monfort, R. Pleixats, L. Rodríguez-Santiago, M. Sodupe, *Chem. Eur. J.* **2013**, *19*, 14553-14565.

[16] M. Gimferrer, P. Salvador, A. Poater, *Organometallics* **2019**, *38*, 4585-4592.

[17] a) A. A. Popov, S. Yang, L. Dunsch, *Chem. Rev.* **2013**, *113*, 5989-6113; b) X. Lu, L. Feng, T. Akasaka, S. Nagase, *Chem. Soc. Rev.* **2012**, *41*, 7723-7760; c) D. M. Rivera-Nazario, J. R. Pinzón, S. Stvenson, L. A. Echegoyen, *J. Phys. Org. Chem.* **2013**, *26*, 194-205; d) M. Rudolf, S. Wolfrum, D. M. Guldi, L. Feng, T. Tsuchiya, T. Akasaka, L. Echegoyen, *Chem. Eur. J.* **2012**, *18*, 5136-5148; e) M. Yamada, T. Akasaka, S. Nagase, *Acc Chem. Res.* **2010**, *43*, 92-102; f) M. N. Chaur, F. Melin, A. L. Ortiz, L. Echegoyen, *Angew. Chem. Int. Ed.* **2009**, *48*, 7514-7538; g) F. Giacalone, N. Martín, *Chem. Rev.* **2006**, *106*, 5136-5190; h) M. Izquierdo, B. Platzer, A. J. Stasyuk, O. A. Stasyuk, A. A. Voityuk, S. Cuesta, M. Solà, D. M. Guldi, N. Martín, *Angew. Chem. Int. Ed.* **2019**, *58*, 6932-6937

[18] a) R. Bakry, R. M Vallant, M. Najam-ul-Haq, M. Rainer, Z. Szabo, C. W. Huck, G. K Bonn, *Int. J. Nanomedicine*. **2007**, *2*, 639-649; b) A. Stoddart, *Nat. Mater.* **2010**, *9*, 876-877.

[19] J. P. Martínez, S. V. C. Vummaleti, L. Falivene, S. P. Nolan, L. Cavallo, M. Solà, A. Poater, *Chem. Eur. J.* **2016**, *22*, 6617-6623.

[20] a) M. A. Mamo, N. J. Coville, W. A. L. van Otterlo, *Fuller. Nanotub. Carbon Nanostructures* **2007**, *15*:5, 341-352; b) Y. N. Biglova, V. V. Mikheev, S. A. Torosyan, R. Z.Biglova, M. S. Miftakhov, *Mendeleev Comm.* **2015**, *25*, 202-203.

[21] B. Hu, T.-X. Liu, P. Zhang, Q. Liu, J. Bi, L. Shi, Z. Zhang, G. Zhang, *Org. Lett.* **2018**, *20*, 4801-4805.

[22] a) M. Chen, L. Bao, M. Ai, W. Shen, X. Lu, *Chem. Sci.* **2016**, *7*, 2331-2334; b) L. Bao, M. Chen, W. Shen, L. Yang, P. Jin, X. Lu, *Inorg. Chem.* **2017**, *56*, 14747-14750; c) M. Chen, W. Shen, P. Peng, L. Ban, S. Zhao, Y. Xie, P. Jin, H. Fang, F.-F. Li, X. Lu, *J. Org. Chem.* **2017**, *82*, 3500-3505; d) P. Jin, L. Yang, C. Liu, M. Chen, Q. Hou, L. Li, Y. Zhao, Phys. Chem. Chem. Phys. **2017**, *19*, 17598-17606.

[23] a) F. L. Bowles, M. M. Olmstead, A. L. Balch, *J. Am. Chem. Soc.* **2014**, *136*, 3338-3341; b) J. P. Martínez, M. Solà, A. Poater, *ChemistryOpen* **2015**, *4*, 774-778; c) M. Nambo, Y. Segawa, A. Wakamiya, K. Itami, *Chem. Asian J.* **2011**, *6*, 590-598; d) N. Martín, M. Altable, S. Filippone, A. Martín-Domenech, A. Poater, M. Solà, *Chem. Eur. J.* **2005**, *11*, 2716-2729; e) J. P. Martínez, M. Vizuete, L. M. Arellano, A. Poater, F. M. Bickelhaupt, F. Langa, M. Solà, *Nanoscale* **2018**, *10*, 15078-15089.

[24] a) V. S. P. K. Neti, M. L. Saha, X. Yan, Z. Zhou, P. J. Stang, *Organometallics* **2015**, *34*, 4813-4815; b) Y. Sun, C. Chen, J. Liu, P. J. Stang, *Chem. Soc. Rev.* **2020**, *49*, 3889-3919.
[25] a) G. Hautier, C. C. Fischer, A. Jain, T. Mueller, G. Ceder, *Chem. Mater.* **2010**, *22*, 3762-3767; b) F. Rissner, Z. Y. Ma, O. T. Hofmann, C. Slugovc, Z. Shuai, E. Zojer, *J. Mater. Chem.* **2012**, *22*, 4269-4272; c) Y. Chu, W. Heyndrickx, G. Occhipinti, V. R. Jensen, B. K. Alsberg, *J. Am. Chem. Soc.* **2012**, *134*, 8885-8895; d) J. Wappel, R. C. Fischer, L. Cavallo, C. Slugovc, A. Poater, *Beilstein J. Org. Chem.* **2016**, *12*, 154-165.
[26] A. Poater, M. C. D'Alterio, G. Talarico, R. Chauvin, *Eur. J. Org. Chem.* **2020**, *2020*, 4743-4749.
[27] A. Poater, E. Pump, S. V. C. Vummaleti, L. Cavallo, *J. Chem. Theory Comput.* **2014**, *10*, 4442-4448.
[28] a) M. Solà, J. Mestres, J. Martí, M. Duran, *Chem. Phys. Lett*. **1994**, *231*, 325-330; b) I. Fernández, M. Solà, F. M. Bickelhaupt, *Chem. Eur. J.* **2013**, *19*, 7416-7422.
[29] a) S. Kozuch, S. Shaik, *J. Phys. Chem. A* **2008**, *112*, 6032-6041; b) A. Uhe, S. Kozuch, S. Shaik, *J. Comput. Chem.* **2011**, *32*, 978-985; c) S. Kozuch, J. M. L. Martin, *ChemPhysChem* **2011**, *12*, 1413-1418; d) S. Kozuch, S. Shaik, *Acc. Chem. Res.* **2011**, *44*, 101-110.
[30] P. Śliwa, M. P. Mitoraj, F. Sagan, J. Handzlik, *J. Mol. Model*. **2019**, *25*, 331.
[31] C. A. Urbina-Blanco, A. Poater, T. Lebl, S. Manzini, A. M. Z. Slawin, L. Cavallo, S. P. Nolan, *J. Am. Chem. Soc.* **2013**, *135*, 7073-7079.
[32] a) E. Pump, A. Poater, N. Bahri-Laleh, R. Credendino, L. Serra, V. Scarano, L. Cavallo, *Catal. Today* **2021**, DOI: 10.1016/j.cattod.2020.04.071; b) A. Poater, L. Cavallo, *Beilstein J. Org. Chem.* **2015**, *11*, 1767-1780.
[33] R. Credendino, A. Poater, F. Ragone, L. Cavallo, *Catal. Sci. Technol.* **2011**, *1*, 1287-1297.
[34] a) X. Solans-Monfort, *Dalton Trans.* **2014**, *43*, 4573-4586; b) A. Poater, X. Solans-Monfort, E. Clot, C. Copéret, O. Eisenstein, *J. Am. Chem. Soc.* **2007**, *129*, 8207-8216.
[35] A. Poater, F. Ragone, A. Correa, L. Cavallo, *Dalton Trans.* **2011**, *40*, 11066-11069.
[36] M. J. S. Dewar, *Bull. Soc. Chim. Fr.* **1951**, *18*, C71-C79.
[37] a) L. M. Azofra, S. V. C. Vummaleti, Z. Zhang, A. Poater, L. Cavallo, *Organometallics* **2020**, *39*, 3972-3982; b) C. P. Gordon, L. Lätsch, C. Copéret, *J. Phys. Chem. Lett.* **2021**, *12*, 2072-2085.
[38] a) L. Cavallo, A. Correa, C. Costabile, H. Jacobsen, *J. Organomet. Chem.* **2005**, *690*, 5407-5413; b) A. Poater, L. Cavallo, *Dalton Trans.* **2009**, 8878-8883.
[39] L. Falivene, R. Credendino, A. Poater, A. Petta, L. Serra, R. Oliva, V. Scarano, L. Cavallo, *Organometallics* **2016**, *35*, 2286-2293.
[40] A. Poater, B. Cosenza, A. Correa, S. Giudice, F. Ragone, V. Scarano, L. Cavallo, *Eur. J. Inorg. Chem.* **2009**, *2009*, 1759-1766.
[41] L. Falivene, Z. Cao, A. Petta, L. Serra, A. Poater, R. Oliva, V. Scarano, L. Cavallo, *Nat. Chem.* **2019**, *11*, 872-879.
[42] a) S. H. Hong, A. Chlenov, M. W. Day, R. H. Grubbs, *Angew. Chem., Int. Ed.* **2007**, *46*, 5148-5151; b) J. Mathew, N. Koga, C. H. Suresh, *Organometallics* **2008**, 27, 4666-4670.
[43] a) D. L. Nascimento, A. Gawin, R. Gawin, P. A. Guńka, J. Zachara, K. Skowerski, D. E. Fogg, *J. Am. Chem. Soc.* **2019**, *141*, 10626-10631; b) S. Manzini, A. Poater, D. J. Nelson, L. Cavallo, A. M. Z. Slawin, S. P. Nolan, *Angew. Chem. Int. Ed.* **2014**, *53*, 8995-8999; c) W. J. van Rensburg, P. J. Steynberg, W. H. Meyer, M. M. Kirk, G. S. Forman, *J. Am. Chem. Soc.* **2004**, *126*, 14332-14333.
[44] a) F. M. Bickelhaupt, *J. Comput. Chem.* **1999**, *20*, 114-128; b) I. Fernández, F. M. Bickelhaupt, *Chem. Soc. Rev.* **2014**, *43*, 4953-4967; c) D. H. Ess, K. N. Houk, *J. Am. Chem. Soc.* **2007**, *129*, 10646-10647; d) W.-J. van Zeist, F. M. Bickelhaupt, *Org. Biomol. Chem.* **2010**, *8*, 3118-3127; e) G. T. de Jong, F. M. Bickelhaupt, *J. Chem. Theory Comput.* **2007**, *3*, 514-529; f) G. T. de Jong, F. M. Bickelhaupt, *ChemPhysChem* **2007**, *8*, 1170-1181; g) L. Zhao, M. von Hopffgarten, D. M. Andrada, Frenking, *Wiley Interdiscip. Rev. Comput. Mol. Sci.* **2018**, *8*, e1345; h) I. Fernández, F. M. Bickelhaupt, F. P. Cossío, *Chem. Eur. J.* **2014**, *20*, 10791-10801.
[45] J. P. Martínez, F. Langa, F. M. Bickelhaupt, S. Osuna, M. Solà, *J. Phys. Chem. C* **2016**, *120*, 1716-1726.
[46] N. Villegas-Escobar, A. Poater, M. Solà, H. F. Schaefer, III, A. Toro-Labbé, *Phys. Chem. Chem. Phys.* **2019**, *21*, 5039-5048.
[47] R. G. Parr, L. v. Szentpály, S. Liu, *J. Am. Chem. Soc.* **1999**, *121*, 1922-1924.
[48] a) P. Geerlings, F. De Proft, W. Langenaeker, *Chem. Rev.* **2003**, *103*, 1793-1874; b) R. G. Parr, R. A. Donnelly, M. Levy, W. E. Palke, *J. Chem. Phys.* **1978**, *68*, 3801; c) R. G. Parr, R. G. Pearson, *J. Am. Chem. Soc.* **1983**, *105*, 7512-7516. d) R. G. Parr, Y. Weitao, *Density-Functional Theory of Atoms and Molecules*, Oxford University Press, New York, **1994**.
[49] T. Koopmans, *Physica* **1934**, *1*, 104-113.
[50] A. Poater, A. Gallegos Saliner, M. Solà, L. Cavallo, A. P. Worth, *Expert Opin. Drug Deliv.* **2010**, *7*, 295-305.
[51] S. Karimi, N. Bahri-Laleh, S. Sadjadi, G. Pareras, M. Nekoomanesh-Haghighi, A. Poater, *J. Ind. Eng. Chem.* **2021**, *97*, 441-451.
[52] Gaussian 09, Revision D.01, M. J. Frisch, G. W. Trucks, H. B. Schlegel, G. E. Scuseria, M. A. Robb, J. R. Cheeseman, G. Scalmani, V. Barone, B. Mennucci, G. A. Petersson, H. Nakatsuji, M. Caricato, X. Li, H. P. Hratchian, A. F. Izmaylov, J. Bloino, G. Zheng, J. L. Sonnenberg, M. Hada, M. Ehara, K. Toyota, R. Fukuda, J. Hasegawa, M. Ishida, T. Nakajima, Y. Honda, O. Kitao, H. Nakai, T. Vreven, J. A. Montgomery, Jr., J. E. Peralta, F. Ogliaro, M. Bearpark, J. J. Heyd, E. Brothers, K. N. Kudin, V. N. Staroverov, R. Kobayashi, J. Normand, K. Raghavachari, A. Rendell, J. C. Burant, S. S. Iyengar, J. Tomasi, M. Cossi, N. Rega, J. M. Millam, M. Klene, J. E. Knox, J. B. Cross, V. Bakken, C. Adamo, J. Jaramillo, R. Gomperts, R. E. Stratmann, O. Yazyev, A. J. Austin, R. Cammi, C. Pomelli, J. W. Ochterski, R. L. Martin, K. Morokuma, V. G. Zakrzewski, G. A. Voth, P. Salvador, J. J. Dannenberg, S. Dapprich, A. D. Daniels, Ö. Farkas, J. B. Foresman, J. V. Ortiz, J. Cioslowski, D. J. Fox, Gaussian, Inc., Wallingford CT, 2009.
[53] Y. Zhao, D. G. Truhlar, *Theor. Chem. Acc.* **2008**, *120*, 215-241.
[54] A. Schaefer, H. Horn, R. Ahlrichs, *J. Chem. Phys*. **1992**, *97*, 2571.
[55] a) U. Häussermann, M. Dolg, H. Stoll, H. Preuss, P. Schwerdtfeger, R, M. Pitzer, *Mol. Phys*. **1993**, *78*, 1211-1224; b) W. Küchle, M. Dolg, H. Stoll, H. Preuss, *J. Chem. Phys*. **1994,** *100*, 7535; c) T. Leininger, A. Nicklass, H. Stoll, *J. Chem. Phys*. **1996**, *105*, 1052.
[56] F. Weigend, R. Ahlrichs, *Phys. Chem. Chem. Phys.* **2005**, *7*, 3297-3305.
[57] a) V. Barone, M. Cossi, *J. Phys. Chem. A* **1998**, *102*, 1995-2001; b) J. Tomasi, M. Persico, *Chem. Rev.* **1994**, *94*, 2027-2094.